Research Article

# Co-substitution of Er/Yb on structural and electrical properties of NKBT–BCZT solid solutions

K. S. K. R. Chandra Sekhar[1] · Kumara Raja Kandula[2] · K. Sowri Babu[3] · N. Narasimha Rao[4] · A. Chitti Babu[5] · K. Chandra Mouli[1] · Tirupathi Patri[6]

Received: 28 July 2019 / Accepted: 13 November 2019 / Published online: 20 November 2019


**Abstract**
Single-phase Er/Yb co-substituted $0.94(Na_{0.4}K_{0.1}Bi_{0.5-x-y}Er_xYb_yTiO_3)-0.06(Ba_{0.85}Ca_{0.15}Zr_{0.1}Ti_{0.9}O_3)$ ($x = 0.01$, $y = 0.02$ and $x = 0.02$, $y = 0.01$) (NKBT–BCZT) lead-free ceramics were synthesized by conventional solid-state reaction. The structural properties of the ceramics were confirmed with the help of X-ray diffraction studies. The crystal structure of NKBT–BCZT changed from rhombohedral to a morphotropic phase boundary and then to tetragonal phase in the presence of BCZT. The surface morphology of these ceramics was well packed with high-density and delineated grain boundaries which were confirmed with the help of the density of the samples. It was noted that the grain sizes decreased slightly by altering the Er/Yb compositions. The temperature dependence dielectric study revealed the existence of ferroelectric and antiferroelectric phase transformations in two independent regions. The temperature dependence conductivity study showed doubly ionized oxygen vacancies due to the presence of a defect dipole, which helps to promote ionic conductivity at a high temperature region. The observed room temperature P–E loops were identified from well-saturated slim loops having reduced coercivity which was found to be useful for potential applications in the field of energy storage devices.

**Keywords** Ferroelectrics · Ceramics · Morphotropic phase · Grain boundary · Conductivity

## 1 Introduction

Lead-free ferroelectrics are promising materials as they replace lead-based materials due to their potential applications in the field of sensors, actuators, motors and memory devices [1–3]. The most widely used piezoelectric ceramics are lead zirconate titanate ($x$) $PbTiO_3 - (1-x)$ $PbZrO_3$ and its solid solutions. Particularly, the solid solution located near the rhombohedral (antiferroelectric $PbZrO_3$)–tetragonal (ferroelectric $PbTiO_3$) is familiar as morphotropic phase boundary (MPB: $x = 0.47$–$0.48$). Near MPB, the material possesses enhanced dielectric constant as well as shows piezoelectric properties such as large electromechanical coupling coefficient ($K_p = 0.70$) and high piezoelectric constant [4, 5].

Pb-based systems are highly toxic and volatile, while sintering process causes serious environmental hazards. Researchers are thus challenged to pay more attention to replace Pb-based ceramics with Pb-free suitable materials without losing their superior properties. In 1960, Smolenskii discovered that sodium bismuth titanate ($Na_{1/2}Bi_{1/2}$) $TiO_3$ [BNT] served as a promising lead-free candidate, containing perovskite structure with A-site disorder [6]. A number of reports on lead-free ferroelectric ceramics

✉ Tirupathi Patri, ptirupathi36@gmail.com | [1]Department of Engineering Physics, A. U. College of Engineering (A), Andhra University, Visakhapatnam 530003, India. [2]St. Martin's Engineering College, Dhullapally, Secunderabad 500100, India. [3]Vignan's Foundation for Science Technology and Research, Vadlamudi, Guntur 522213, India. [4]PACE Institution of Technology and Science, Ongole 523273, India. [5]Department of Physics, Rajiv Gandhi University of Knowledge Technologies (AP – IIIT), Nuziveedu 521201, India. [6]Department of Physics, Rajiv Gandhi University of Knowledge Technologies (AP – IIIT), RK Valley, Kadapa 516330, India.

are mentioned in the literature [7–9]. Therefore, it has been considered to be a suitable material to replace lead-based piezoelectric ceramic because of its good ferroelectric properties [remnant polarization $P_r = 38$ μC/cm$^2$ at room temperature (RT)] and at a high Curie temperature ($T_c = 320$ °C) [10]. It exhibits a rhombohedral perovskite-like structure and shows an anomaly in dielectric properties as a result of a low-temperature phase transition from the ferroelectric to antiferroelectric phase at ~ 200 °C (known as depolarization temperature $T_d$) [11, 12]. On the other hand, high leakage current during poling with low field hampers incomplete polarization loops. In order to obtain useful lead-free piezoelectric ceramics, BNT-based compositions have been modified with $BaTiO_3$ [11], $(Bi_{1/2}K_{1/2})TiO_3$ [12], $NaNbO_3$ [13], $BiFeO_3$ [14, 15], $Bi_2O_3$–$Sc_2O_3$ [16] and $Ba(Cu_{1/2}W_{1/2})O_3$ [17]. Reports showed an improvement in either ways i.e., easier to pole, or have enhanced piezoelectric properties as compared with pure BNT ceramics.

Liu and Ren et al. reported outstanding piezoelectric properties with large dielectric constant on $x$Ba$(Zr_{0.2}Ti_{0.8})O_3 - (1-x)(Ba_{0.7}Ca_{0.3})TiO_3$, $(x = 0.5)$ BZT–BCT ceramics with conventional solid-state route. The high piezoelectric effect can be attributed to the MPB, which stared from a tetragonal–cubic–rhombohedral triple point which caused a very low energy barrier for polarization rotation and lattice distortion [18]. Although it has high calcination and sintering temperatures, i.e., well above > 1300 °C ~ 1500 °C, the synthesis process is at normal conditions. The wet chemical processes, such as sol–gel, hydrothermal, Pechini and sol–gel autocombustion methods, are used to prepare BCZT powders [19]. The properties change of piezoelectric materials is preparation dependent; so much attention has been paid to the synthesis of BCZT ceramics. Recently, an environment-friendly lead-free $[(Ba_{0.85}Ca_{0.15})(Zr_{0.1}Ti_{0.9})O_3]$ system attracted much attention due to its extraordinarily high piezoelectric properties ($d_{33}$ ~ 620 pC/N). The polarization versus electric field measurements were traced for $Ba_{0.85}Ca_{0.15}Zr_{0.1}Ti_{0.9}O_3$ sample which showed a remnant polarization ($P_r$) of 11.55 μC/cm$^2$ and a coercive field ($E_c$) of 0.166 kV/cm [20]. Here, the $Yb^{3+}/Er^{3+}$ substitution which alters the compositions mainly is because of the close ionic radii of Bi and also the additive functionality of the upconversion mechanism will be explained in further communications. We prepared co-substitution of rare earth $Yb^{3+}/Er^{3+}$ at Bi-site in $0.94(Na_{0.4}K_{0.1}Bi_{0.5-x-y}Er_xYb_yTiO_3)$–$0.06(Ba_{0.85}Ca_{0.15}Zr_{0.1}Ti_{0.9}O_3)$ ($x = 0.01$, $y = 0.02$ and $x = 0.02$, $y = 0.01$). ($x = 0.02$, $y = 0.01$ abbreviated as NKBT–BCZT-1 and $x = 0.01$, $y = 0.02$ abbreviated as NKBT–BCZT-2) ceramics, respectively. Here in this present paper, we have reported the effect of $Yb^{3+}/Er^{3+}$ ion at Bi-site in structural analysis with the help of room temperature XRD. The detailed microstructure, polarization studies, energy density calculations are also reported. Besides this, a detailed temperature-dependent dielectric phase transition and conductivity studies are also reported.

## 2 Materials and methods

The NKBT–BCZT solid solutions were prepared by using conventional solid-state reaction method in two steps. The first step $Ba_{0.85}Ca_{0.15}Zr_{0.1}Ti_{0.9}O_3$ was prepared by using high-purity analytical reagent (AR) grade using $BaCO_3$, $CaCO_3$, $ZrO_2$ and $TiO_2$ as starting materials. The raw powders were weighed as per the stoichiometric ratio, mixed, grounded in agate mortar in 2-propanol medium for 3–4 h and then calcined at 1000 °C for 3 h. In the second step, $Na_{0.4}K_{0.1}Bi_{0.5-x-y}Er_xYb_yTiO_3$ were prepared with the help of pure A.R grade $Bi_2O_3$, $Na_2CO_3$, $K_2CO_3$, $TiO_2$, $Er_2O_3$, $Yb_2O_3$ which were used as raw materials. The powders were weighed, mixed well and grounded in an agate mortar in 2-propanol as medium for 4 h. The calcination was then carried out at 800 °C for 3 h.

The two calcined and finely grounded powders were mixed as per the stoichiometric ratio for the compounds $0.94(Na_{0.4}K_{0.1}Bi_{0.5-x-y}Er_xYb_yTiO_3)$–$0.06(Ba_{0.85}Ca_{0.15}Zr_{0.1}Ti_{0.9}O_3)$. The fine powders were then pressed into pellets with about 1 mm thickness and diameter of 10 mm. The samples were sintered at 1150 °C for 3 h at a heating rate 5 °C/min. The structural phase purity and the formation of perovskite phase of these ceramics were examined by using XRD ranging between $20° \leq 2\theta \leq 80°$ with the help of X-ray diffractometer of PHILIPS-PW3373 XPERT-PRO with CuKα radiation ($\lambda = 1.5405$ Å). The surface morphology of these sintered samples was examined by using field emission scanning electron microscope (FESEM) with the model of Carl Zeiss Supra SEM 40. The room temperature (RT) ferroelectric hysteresis loops were measured using a standard radiant Sawyer–Tower circuit radiant analyzer. The high-temperature dielectric measurements were taken by using an impedance analyzer of model no: HP 4192A in the frequency range from 100 Hz to 1 MHz, while keeping the electrode of silver paste pellets in sandwich geometry.

## 3 Results and discussion

### 3.1 X-ray diffraction analysis

Figure 1a shows the room temperature XRD pattern of NKBT–BCZT-1, NKBT–BCZT-2 sintered ceramics within the range of $20° \leq 2\theta \leq 80°$. The structural data showed a pure perovskite structure without the coexistence of secondary phases. This was observed from the ceramic samples that structural phase purity while the substitution of

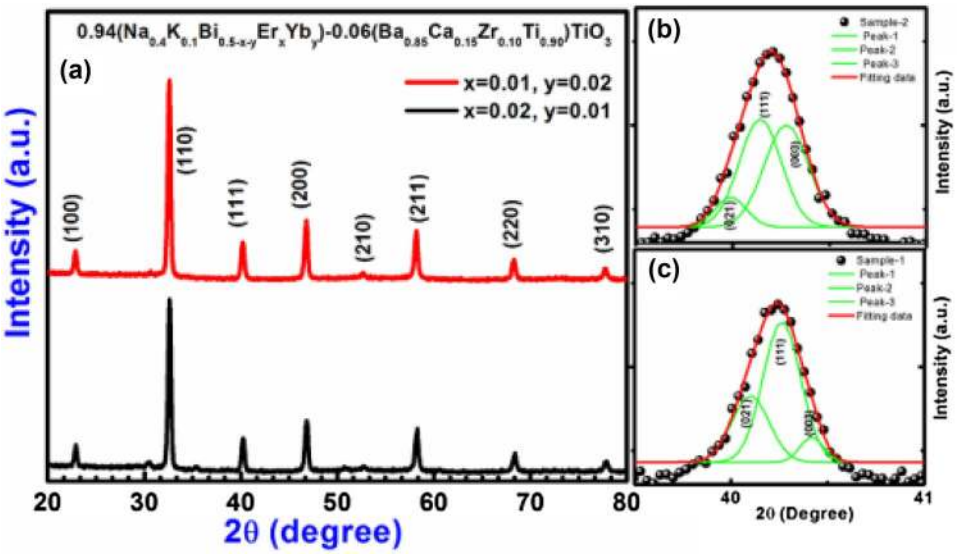


**Fig. 1** Room temperature powder X-ray diffraction patterns of NKBT–BCZT, **b**–**c** Lorentzian–Gaussian peak fit at $39° \leq 2\theta \leq 41°$ region at plane (111) (012)/(003)

Er and Yb at Bi-site diffuses completely. The RT structure of NKBT is rhombohedral with R3c; on the other hand, BCZT is tetragonal with P4 mm phase. No considerable changes were observed in the peak profile, such as shifting and the shape of the Bragg's reflection to alter the Er and Yb. As per reports for NKBT–BCZT-1, two solid solutions might coexist in dual structural phase with major rhombohedral R3c along with minor tetragonal P4 mm. Further, the coexistence of tetragonal reflections along with major rhombohedral reflections was observed from the deconvolution of Bragg's reflection of $(111)_{pc}$, which deconvoluted into (012)/(003) peaks near $39° \leq 2\theta \leq 41°$ regimes shown in Fig. 1b, c. These observations confirmed the possibility of coexistence of dual structural phases, R3c + P4 mm model. Further, the confirmation of structural coexistence of dual structural phase being analyzed in detail by Rietveld refinement is under progress.

### 3.2 Microstructural analysis

Figure 2a, b shows the surface morphology of NKBT–BCZT-1 and NKBT–BCZT-2 ceramics. The grain boundaries are well delineated, and no phase segregation at grain boundaries was observed, which revealed negligible porosity and also reflected its high density. The average grain size of these dense ceramics was calculated by using linear intercepts method, and it was observed that the average grain size decreased slightly from 0.9 to 0.8 µm in the presence of concentration change of Er/Yb. The change in the composition leads to a decrease in the grain size slightly. The reduction in grain size and proper connectivity of the grains leads to reduce the porosity of the specimens. This porosity reduction helps to enhance the density beneficial to achieve large breakdown strength and high energy storage. The solidity and slight variation in grain size can be explained in view of induced strain in the interior of grain and grain boundary due to slight

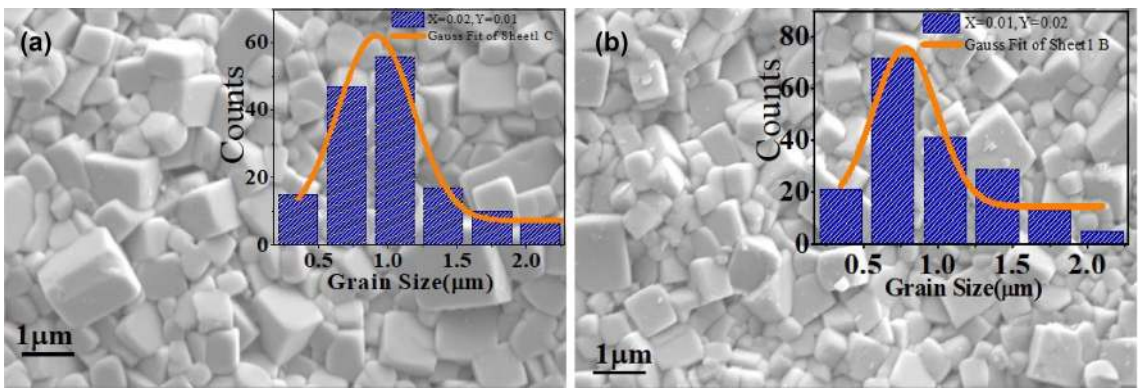


**Fig. 2** **a**, **b** Surface morphology of NKBT–BCZT sintered ceramics shows from (**a**, **b**) along with average grain distribution curve

mismatch in ionic radii of constituting element in the present ceramics. The grain size distribution of NKBT–BCZT ceramics is shown in Fig. 2a, b with the help of Gaussian distribution function.

### 3.3 Ferroelectric and energy storage measurements

Figure 3a, b, shows the polarization V/s electric field (P–E) hysteresis loops, which were measured at RT for both ceramics under different electric fields. The polarization loops of the ceramics showed well-saturated and typical soft ferroelectric behavior with low coercive fields. The slanted slim behavior of the loops indicates the domain structure of the ceramics which undergoes a macro- to micro-domain evolution. The ceramics with high remanent polarization ($P_r$) are not favorable to high energy storage applications. The noted P-E loop of the given ceramics with good saturation polarization ($P_s$) and low $P_r$ values which were achieved especially due to alter the compositions Er/Yb were beneficial for the energy storage applications. The energy storage density of these ceramics estimated from the polarization loops, during the discharge process, was calculated by using the following relation 1 [21].

$$E_{stor} = \int_{P_r}^{P\max} EdP \quad (1)$$

Here $E$ is the electric field, and $P_{max}$ is the maximum polarization during the charging process and $P_r$ is the remnant polarization.

It is noted that the calculated recoverable energy storage values increase with increasing applied fields. The evaluation of recoverable energy storage density was calculated by integrating the area of first quadrant between the polarization axis and the discharge curve. It could have

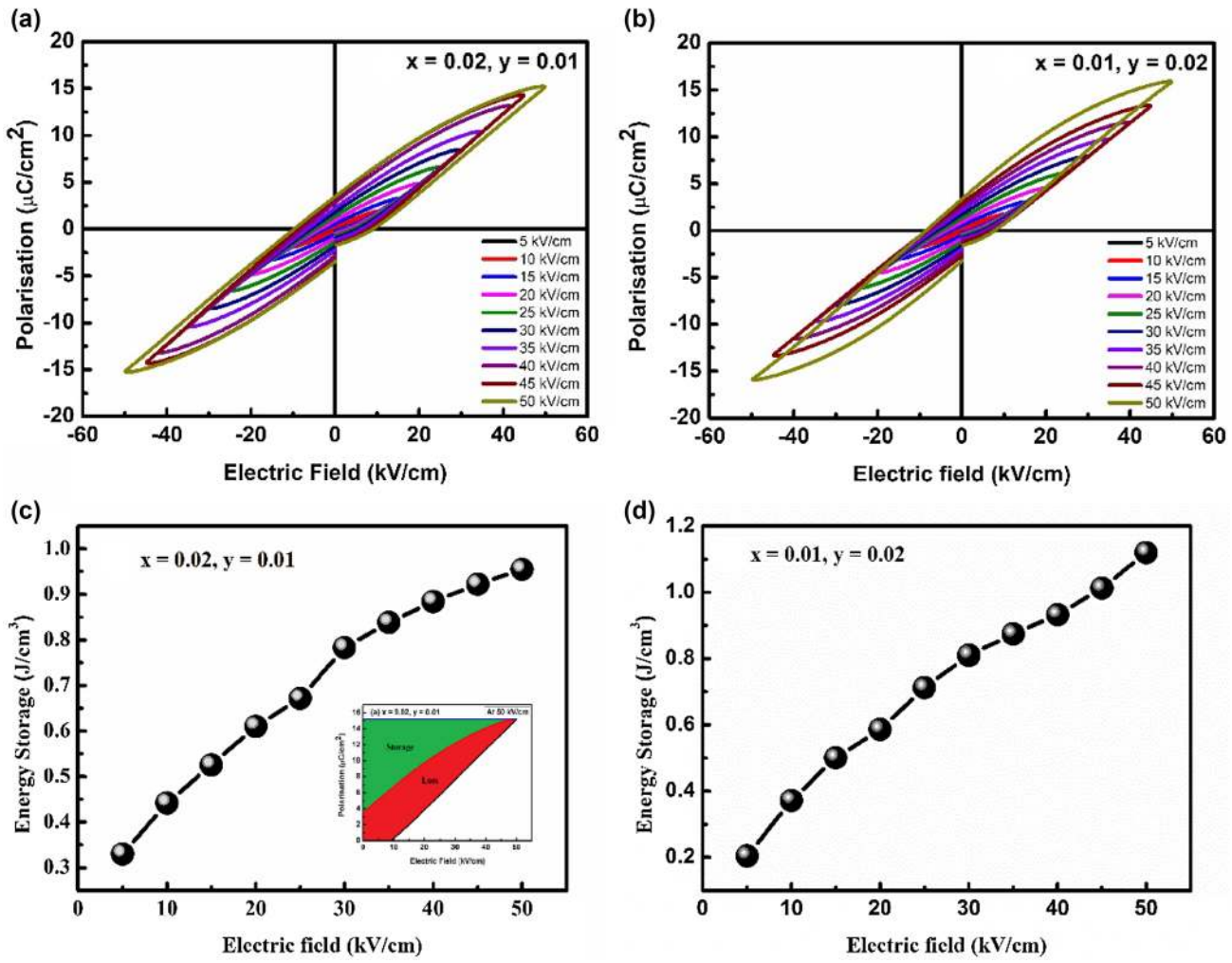


**Fig. 3** **a**, **b** RT P–E hysteresis loops of NKBT–BCZT ceramics at various electric fields. **c**, **d** The energy storage with the variation of field for both the ceramics. Inset **c** shows the schematic view energy storage and energy loss for ceramics 1 at field 50 kV/cm

been a much higher energy storage density at maximum field at 50 kV/cm. The estimated energy storage values for ceramics 1 and ceramics 2 were found to be 0.93 J/cm$^3$ and 1.12 J/cm$^3$, respectively, at field strength 50 kV/cm. These estimated values are well and slightly lower than that of NBT–BT-based ceramics, which are in good agreement with recently reported BT-based ceramics [22, 23]. The slight variation in energy storage density could be explained due to its submicron grain size and high relative density which increased with concentration $Er^{3+}$. Thus, these ceramics are promising materials for energy storage capacitor dielectrics [24, 25].

### 3.4 Temperature-dependent dielectric studies

Temperature-dependent dielectric permittivity and loss (tanδ) study in fixed frequency intervals (100 Hz–1 MHz) and temperature (30–500 °C) range were carried out and are shown in Fig. 4a, b. Ceramics 1 ($x = 0.02,\ y = 0.01$) depicts dielectric constant ($\varepsilon_r$) ~ 112 at frequency of 10 kHz near RT, whereas ceramics 2 ($x = 0.01,\ y = 0.02$) exhibits large dielectric permittivity ($\varepsilon_r$) ~ 396 at RT. Here both the ceramics relative part of dielectric $\varepsilon_r(T)$ plot exhibits two sets of dielectric phase transitions at 150–160 °C and 270–290 °C intervals, respectively. Usually, the low region dielectric phase transition peaks are denoted as depolarization ($T_d$), which are responsible for the ferroelectric–antiferroelectric transition. The second phase transition observed at the high temperature region is denoted as ($T_c$), which is responsible for the antiferroelectric to paraelectric phase transition where the material acquires maximum dielectric constant. For ceramics 1 ($x = 0.02,\ y = 0.01$), the noted ($T_d$) and ($T_c$) are 165 °C, 289 °C, and for ceramics 2 ($x = 0.01,\ y = 0.02$) they are 159 °C, 280 °C, respectively. The observed values are in good agreement with recent reports [26, 27]. The slight variation in phase transitions toward lower temperature with interchange in composition ratios due to strong hybridization between $Bi^{3+}$ and $Er^{3+}$ with increment in Er substitution NKBT–BCZT ceramics, leads to more stability toward ferroelectric domains in ($x = 0.02,\ y = 0.01$) ceramics 2. On the other hand, the observed $T_c$ shifts toward a lower temperature, while $Er^{3+}$ increment indicates the stability of ferroelectric domain in the long range. Yb seems to act as a strong suppressor of the dielectric peak between antiferroelectric and paraelectric, but as a weak promoter of the dielectric shoulder between ferroelectric and antiferroelectric [28]. Besides the shifting of dielectric phase transitions ($T_d$ and $T_c$), there was a significant modification in the dielectric constant as well as dielectric loss parameters in ceramics 2. The phase transition modification mainly exhibits a strong hybridization between $Bi^{3+}$–O–$Er^{3+}$ rather than with $Bi^{3+}$–O–$Yb^{3+}$ which

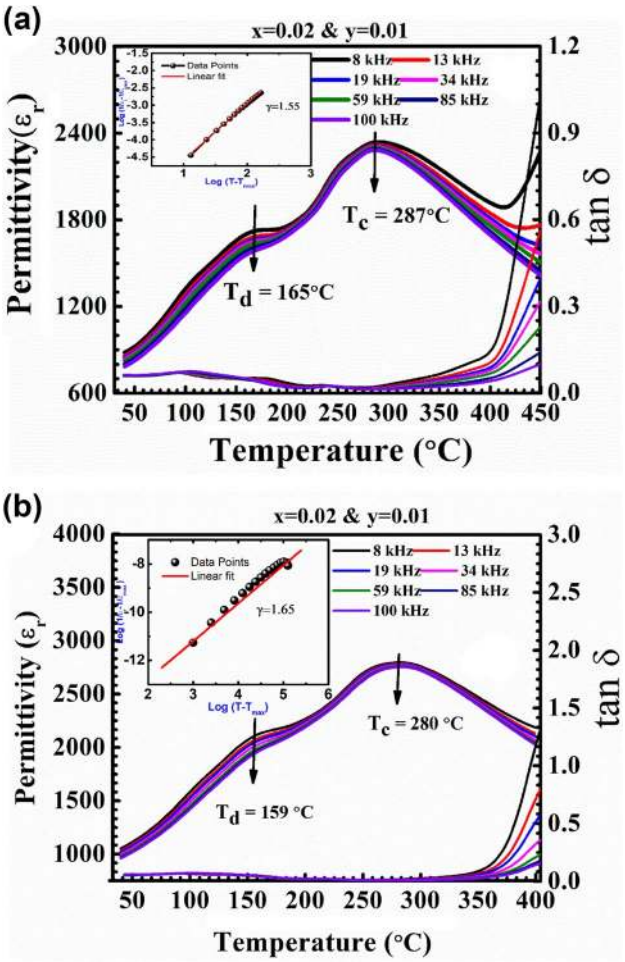


**Fig. 4** **a**, **b** Variation of dielectric permittivity with temperature range 30–500 °C within the frequency intervals 100 Hz–1 MHz. Inset figure shows the diffusivity to reflects the relaxor nature of the both ceramic

could lead to an increase in the dielectric constant [29, 30]. The substitution of $Er^{3+}$ in NKBT–BCZT ceramics showed dielectric constant ($\varepsilon_r$) ~ 396 as well as dielectric loss at RT, which indicated that $Er^{3+}$ substitution leads to decrease in conductivity. The left side of Fig. 4a, b shows an enormous dielectric loss from tanδ (imaginary part) plot that also exhibits frequency dispersion at high temperature which is depicted like a normal of a well-known classical diffused relaxor ferroelectric material [30, 31]. In addition, the broadness of the $T_c$ at high temperature was noted for both ceramics. In order to understand the relaxor activity, we plotted $\log(1/\varepsilon - 1/\varepsilon_{max})$ v/s $\log(T - T_{max})$, which represents the value of γ, which is 1 for the case of a normal ferroelectric and a quadratic (i.e., $\gamma = 2$) is valid for a relaxor with diffused ferroelectric material. From the graph, the estimated diffusivity (γ) was found to be 1.55 and 1.65 for ceramics 1 and ceramics 2, respectively. The observed (γ)

values well matched with known classical relaxor diffused ferroelectric materials [31, 32].

The relaxor activity and asymmetric nature of slim curves are indicated with the help of bipolar strain v/s electric field (S–E) loops. Both the ceramics exhibits an asymmetric butterfly-shaped feature due to the existence of an internal bias field which is associated with the motion of domains and domain walls [33] as shown in Fig. 5a, b with maximum field of 60 kV/cm. The observed maximum strain ($S_{max}$) = 0.10% for ceramics 2 represents both its magnitude (positive and negative), thereby indicating its relaxor nature. In case of ceramics 1, a slight decrease and eventually vanishing negative strain region were observed with maximum value 0.95% [34, 35]. The measured standards from the strain have been well synchronized with P–E loops, which represent the diffused relaxor ferroelectric behavior for $Yb^{3+}/Er^{3+}$ substituted in NKBT–BCZT ceramics. Hence, the substitution of $Yb^{3+}/Er^{3+}$ in NKBT–BCZT showed that the diffuse relaxor ferroelectric character can be useful for future applications in energy storage devices.

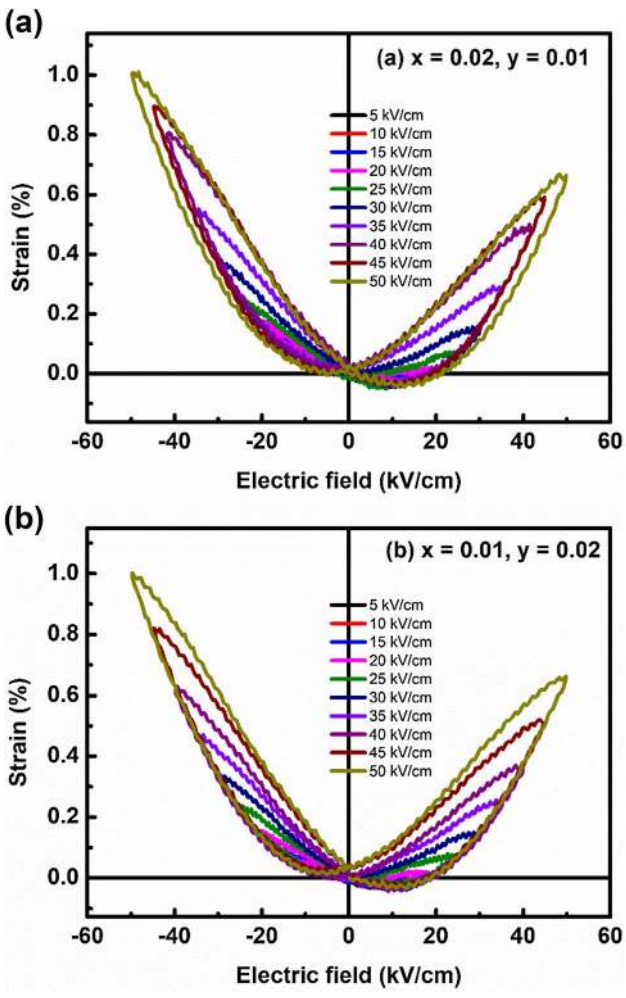


**Fig. 5** **a**, **b** Variation of bipolar strain with electric field in fixed loop frequency of 1 Hz

### 3.5 Temperature-dependent conductivity studies

To elaborate the dielectric relaxation mechanism associated with temperature and corresponding charge species involved in the conduction process, we have measured the temperature dependence of the AC conductivity in fixed frequencies by using the following formula.

$$\sigma_{ac} = \omega \varepsilon_r \varepsilon_0 \tan \delta \quad (2)$$

where $\sigma_{ac}$ = AC conductivity, $\varepsilon_r$ = relative dielectric constant, $\varepsilon_0$ = dielectric permittivity in vacuum, ω is angular frequency, and tanδ is loss factor [36]. It was found that the conductivity is of the order $5.5 \times 10^{-6}$ S/m for ceramics 1 and $2.1 \times 10^{-5}$ S/m for ceramics 2 at RT and at 10 kHz frequency. The noted values were found to be in good agreement with its semiconducting nature. Furthermore, it was observed that conductivity strongly depends upon the frequency by the variation of temperature. A certain temperature showed a short plateau region, above 300 °C, and then, a sudden rise in conductivity was noted. The sudden rise in conductivity at high temperature was studied by plotting the variation of conductivity with reciprocal of temperature as shown in Fig. 6a, b. It is well fitted with the Arrhenius relation:

$$\sigma = \sigma_0 \exp\left(-\Delta E_a / k_B T\right) \quad (3)$$

where $E_a$, $k_B$, $T$ bear their usual meanings, and the noted value of activation energy was found to be $E_a$ = 0.65 eV for ceramics 1 and $E_a$ = 0.83 eV for ceramics 2 in region above 300 °C. These noted values are in good agreement with the single ionized oxygen vacancies dominated due to defect in dipoles or ionic conduction which are commonly present in perovskite structures [37, 38]. The observed results suggest that the hopping conduction through oxygen vacancies is responsible for conductivity at high temperature. Also, the motion of oxygen vacancies is well known to give rise to activation energy of about 1 eV at high temperatures in perovskite oxides [39]. One should also presume that other point defects and cationic disorder contribute toward DC conductivity in addition to oxygen vacancies [37, 38].

## 4 Conclusion

The XRD pattern of $Er^{3+}$ and $Yb^{3+}$ co-substituted NKBT–BCZT solid solutions revealed coexistence of dual phases (R3c + P4 mm) for both ceramics, respectively. The

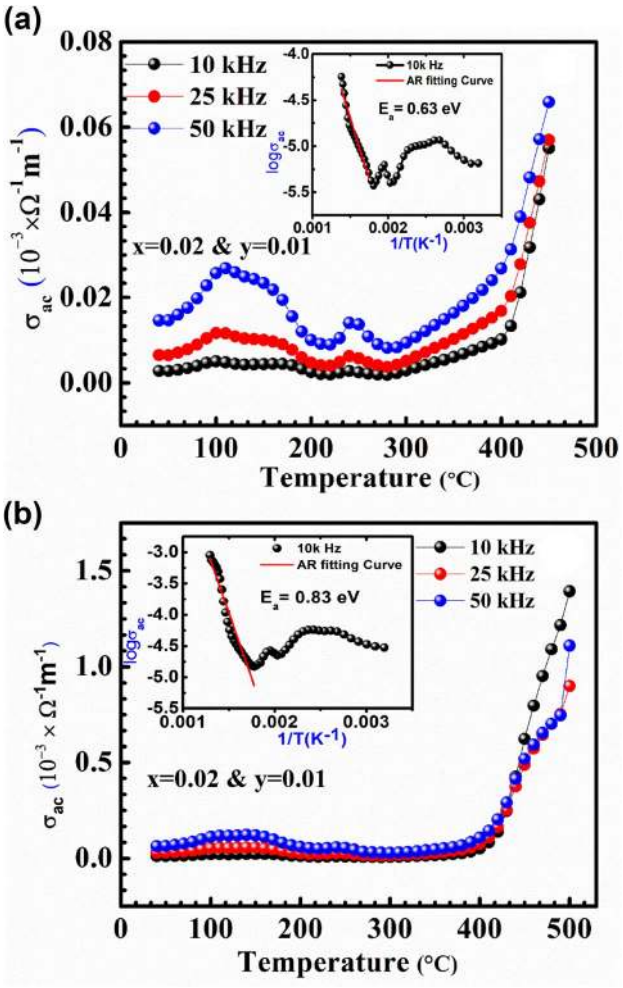


**Fig. 6** **a**, **b** Variation of AC conductivity with temperature range 30–500 °C from the frequency 10 to 50 kHz for ceramic samples 1 and 2, respectively. The inset figure shows the activation energy for both the ceramics

temperature-dependent dielectric studies revealed $T_d$ (depolarization) and $T_c$ (Curie temperature) phase transitions at 160 to 170 °C and 280 to 290 °C, respectively, in both the ceramics. With increasing $Er^{3+}$ concentration, a slight shift of $T_m$ toward high temperature and large decrement in RT dielectric constant were observed. It was found that the NKBT–BCZT-2 sample has high conductivity and high activation energy compared with another sample. The high conductivity in NKBT–BCZT-2 could be the development of anion vacancies with the substitution of $Ba^{2+}$, $K^+$, $Ca^{2+}$, $Er^{3+}$ and $Yb^{3+}$ ions at $Na^+$ and $Bi^{3+}$ ions in the NBT lattice. The present ceramics show good energy storage density as well as enhancement by ~ 21% by altering the substitution of Er and Yb substitution.

**Acknowledgements** The authors would like to thank UGC-DAE Consortium, Mumbai Centre, India, for providing experimental facilities and financial support under UGC-DAE, CRS-M-216-Sponsored Project Scheme.

## Compliance with ethical standards

**Conflict of interest** The authors declare that they have no conflict of interest.

## References

1. Jaffe B, Cook WR, Jaffe H (1971) Piezoelectric ceramics. In: Roberts JP, Popper P (eds) Non metallic solid. Academic Press, London, p 91
2. Haertling GH (1999) Ferroelectric ceramics: history and technology. J Am Ceram Soc 82(4):797–818. https://doi.org/10.1111/j.1151-2916.1999.tb01840.x
3. Bellaiche L (2002) Piezoelectricity of ferroelectric perovskites from first principles. Curr OpinSolid State Mater Sci 6(1):19–25. https://doi.org/10.1016/s1359-0286(02)00017-7
4. Noheda B, Cox DE, Shirane G, Gonzalo JA, Cross LE, Park SE (1999) A monoclinic ferroelectric phase in the $Pb(Zr_{1-x}Ti_x)O_3$ solid solution. Appl Phys Lett 74(14):2059–2061. https://doi.org/10.1063/1.123756
5. Heywang W, Lubitz K, Wersing W (eds) (2008) Piezoelectricity: evolution and future of a technology, vol 14. Springer, Berlin. https://doi.org/10.1007/978-3-540-68683-5
6. Smolensky GA (1961) New ferroelectrics of complex composition. IV. Sov Phys Solid State 2:2651–2654
7. Suchanicz J, Roleder K, Kania A, Hańaderek J (1988) Electrostrictive strain and pyroeffect in the region of phase coexistence in $Na_{0.5}Bi_{0.5}TiO_3$. Ferroelectrics 77(1):107–110. https://doi.org/10.1080/00150198808223232
8. Zvirgzds JA, Kapostin PP, Zvirgzde JV, Kruzina TV (1982) X-ray study of phase transitions in ferroelectric $Na_{0.5}Bi_{0.5}TiO_3$. Ferroelectrics 40(1):75–77. https://doi.org/10.1080/00150198208210600
9. Roleder K, Franke I, Glazer AM, Thomas PA, Miga S, Suchanicz J (2002) The piezoelectric effect in $Na_{0.5}Bi_{0.5}TiO_3$ ceramics. J Phys: Condens Matter 14(21):5399. https://doi.org/10.1088/0953-8984/14/21/314
10. Jones GO, Thomas PA (2002) Investigation of the structure and phase transitions in the novel A-site substituted distorted perovskite compound $Na_{0.5}Bi_{0.5}TiO_3$. Acta Crystallogr Sect B: Struct Sci 58(2):168–178. https://doi.org/10.1107/S0108768101020845
11. Takenaka T, Maruyama KI, Sakata K (1991) $(Bi_{1/2}Na_{1/2})$ TiO3–$BaTiO_3$ system for lead-free piezoelectric ceramics. Jpn J Appl Phys 30(9S):2236. https://doi.org/10.1143/JJAP.30.2236
12. Sasaki A, Chiba T, Mamiya Y, Otsuki E (1999) Dielectric and piezoelectric properties of $(Bi_{0.5}Na_{0.5})TiO_3$–$(Bi_{0.5}K_{0.5})TiO_3$ systems. Jpn J Appl Phys 38(9S):5564. https://doi.org/10.1143/jjap.38.5564
13. Takenaka T, Okuda T, Takegahara K (1997) Lead-free piezoelectric ceramics based on $(Bi_{1/2}Na_{1/2})$ $TiO_3$–$NaNbO_3$. Ferroelectrics 196(1):175–178. https://doi.org/10.1080/00150199708224156
14. Badapanda T, Venkatesan S, Panigrahi S, Kumar P (2013) Structure and dielectric properties of bismuth sodium titanate ceramic prepared by auto-combustion technique. Process Appl Ceram 7(3):135–141. https://doi.org/10.2298/pac1303135b
15. Wu M, Fang L, Liu L, Li G, Elouadi B (2015) Dielectric and ferroelectric properties of $(1-x)$ $BiFeO_3$–$x$ $Bi_{0.5}Na_{0.5}TiO_3$ solid solution. Ferroelectrics 478(1):18–25

16. Nagata H, Takenaka T (1997) Lead-free piezoelectric ceramics of $(Bi_{1/2}Na_{1/2})TiO_3$–$1/2(Bi_2O_3{\cdot}Sc_2O_3)$ system. Jpn J Appl Phys 36(9S):6055–6057. https://doi.org/10.1143/jjap.36.6055
17. Wang X, Chan HL, Choy CL (2003) $(Bi_{1/2}Na_{1/2})TiO_3$–$Ba(Cu_{1/2}W_{1/2})O_3$ lead-free piezoelectric ceramics. J Am Ceram Soc 86(10):1809–1811. https://doi.org/10.1111/j.1151-2916.2003.tb03562.x
18. Liu W, Ren X (2009) Large piezoelectric effect in Pb-free ceramics. Phys Rev Lett 103(25):257602. https://doi.org/10.1103/physrevlett.103.257602
19. Sahoo GK, Mazumder R (2014) Low temperature synthesis of $Ba(Zr_{0.2}Ti_{0.8})O_3$–$0.5(Ba_{0.7}Ca_{0.3})TiO_3$ nanopowders by solution based auto combustion method. J Mater Sci Mater Electron 25(8):3515–3519. https://doi.org/10.1007/s10854-014-2048-2
20. Praveen JP, Kumar K, James Raju CK, Das D (2013) A study of piezoelectric properties of $(Ba_{0.85}Ca_{0.15})(Zr_{0.9}Ti_{0.1})O_3$ ceramics synthesized by sol–gel process. In: AIP conference proceedings 1536(1), 891–892. https://doi.org/10.1063/1.4810515
21. Chauhan A, Patel S, Vaish R (2014) Mechanical confinement for improved energy storage density in BNT-BT-KNN lead-free ceramic capacitors. AIP Adv 4(8):087106. https://doi.org/10.1063/1.4892608
22. Shen Z, Wang X, Luo B, Li L (2015) $BaTiO_3$–$BiYbO_3$ perovskite materials for energy storage applications. J Mater Chem A 3(35):18146–18153. https://doi.org/10.1039/c5ta03614c
23. Cao W, Li W, Zhang T, Sheng J, Hou Y, Feng Y, Yu Y, Fei W (2015) High-energy storage density and efficiency of $(1-x)$[0.94 NBT–0.06 BT]–xST lead-free ceramics. Energy Technol 3(12):1198–1204. https://doi.org/10.1002/ente.201500173
24. Cao WP, Li WL, Dai XF, Zhang TD, Sheng J, Hou YF, Fei WD (2016) Large electrocaloric response and high energy-storage properties over a broad temperature range in lead-free NBT-ST ceramics. J Eur Ceram Soc 36(3):593–600. https://doi.org/10.1016/j.jeurceramsoc.2015.10.019
25. Li L, Xu M, Zhang Q, Chen P, Wang N, Xiong D, Peng B, Liu L (2018) Electrocaloric effect in La-doped BNT-6BT relaxor ferroelectric ceramics. Ceram Int 44(1):343–350
26. Liu L, Ma X, Knapp M, Ehrenberg H, Peng B, Fang L, Hinterstein M (2017) Thermal evolution of polar nanoregions identified by the relaxation time of electric modulus in the $Bi_{1/2}Na_{1/2}TiO_3$ system. EPL (Europhys Lett) 118(4):47001
27. Chandrasekhar M, Kumar P (2016) Synthesis and characterizations of BNT–BT–KNN ceramics for energy storage applications. Phase Transit 89(9):944–957. https://doi.org/10.1080/01411594.2015.1118763
28. Han F, Deng J, Liu X, Yan T, Ren S, Ma X, Liu S, Peng B, Liu L (2017) High-temperature dielectric and relaxation behavior of Yb-doped $Bi_{0.5}Na_{0.5}TiO_3$ ceramics. Ceram Int 43(7):5564–5573
29. Ogihara H, Randall CA, Trolier-McKinstry S (2009) High-energy density capacitors utilizing $0.7BaTiO_3$–$0.3BiScO_3$ ceramics. J Am Ceram Soc 92(8):1719–1724. https://doi.org/10.1111/j.1551-2916.2009.03104.x
30. Tian HY, Wang DY, Lin DM, Zeng JT, Kwok KW, Chan HL (2007) Diffusion phase transition and dielectric characteristics of $Bi_{0.5}Na_{0.5}TiO_3$–$Ba(Hf,Ti)O_3$ lead-free ceramics. Solid State Commun 142(1–2):10–14. https://doi.org/10.1016/j.ssc.2007.01.043
31. Uchino K, Nomura S, Cross LE, Jang SJ, Newnham RE (1980) Electrostrictive effect in lead magnesium niobate single crystals. J Appl Phys 51(2):1142–1145. https://doi.org/10.1063/1.327724
32. Shannigrahi S, Choudhary RN, Acharya HN, Sinha TP (1999) Phase transition in sol–gel-derived Na-modified PLZT ceramics. J Phys D Appl Phys 32(13):1539. https://doi.org/10.1088/0022-3727/32/13/315
33. Liu L, Shi D, Knapp M, Ehrenberg H, Fang L, Chen J (2014) Large strain response based on relaxor-antiferroelectric coherence in $Bi_{0.5}Na_{0.5}TiO_3$–$SrTiO_3$–$(K_{0.5}Na_{0.5})NbO_3$ solid solutions. J Appl Phys 116(18):184104
34. Ullah A, Ahn CW, Lee SY, Kim JS, Kim IW (2012) Structure, ferroelectric properties, and electric field-induced large strain in lead-free $Bi_{0.5}(Na,K)_{0.5}TiO_3$–$(Bi_{0.5}La_{0.5})AlO_3$ piezoelectric ceramics. Ceram Int 38:S363–S368. https://doi.org/10.1016/j.ceramint.2011.05.013
35. Zhang ST, Kounga AB, Aulbach E, Granzow T, Jo W, Kleebe HJ, Rödel J (2008) Lead-free piezoceramics with giant strain in the system $Bi_{0.5}Na_{0.5}TiO_3$–$BaTiO_3$–$K_{0.5}Na_{0.5}NbO_3$, structure and room temperature properties. J Appl Phys 103(3):034108. https://doi.org/10.1063/1.2838476
36. Patri T, Justin P, Babu PD, Ghosh A (2019) Analysis of dielectric and magnetic phase transitions in $Yb(Fe_{0.5}Cr_{0.5})O_3$ bulk perovskite. Appl Phys A 125(4):224. https://doi.org/10.1007/s00339-019-2516-x
37. Li M, Zhang H, Cook SN, Li L, Kilner JA, Reaney IM, Sinclair DC (2015) Dramatic influence of A-site nonstoichiometry on the electrical conductivity and conduction mechanisms in the perovskite oxide $Na_{0.5}Bi_{0.5}TiO_3$. Chem Mater 27(2):629–634. https://doi.org/10.1021/cm504475k
38. Sun Y, Liu H, Hao H, Zhang S (2016) Effect of oxygen vacancy on electrical property of acceptor doped $BaTiO_3$–$Na_{0.5}Bi_{0.5}TiO_3$–$Nb_2O_5$ X8R systems. J Am Ceram Soc 99(9):3067–3073. https://doi.org/10.1111/jace.14336
39. Yan T, Sun X, Deng J, Liu S, Han F, Liu X, Fang L, Lin D, Peng B, Liu L (2017) Dielectric and conductivity behavior of Mn-doped $K_{0.5}Na_{0.5}NbO_3$ single crystal. Solid State Commun 264:1–5